FEBS Letters 581 (2007) 2905–2913

Quantitative single particle tracking of NGF–receptor complexes: Transport is bidirectional but biased by longer retrograde run lengths

María M. Echarte[a], Luciana Bruno[b,d], Donna J. Arndt-Jovin[c], Thomas M. Jovin[c], Lía I. Pietrasanta[a,d,*]

[a] *Centro de Microscopías Avanzadas, Facultad de Ciencias Exactas y Naturales, Universidad de Buenos Aires, Intendente Güiraldes 2160, Pabellón I, Ciudad Universitaria, C1428EHA Buenos Aires, Argentina*
[b] *Departamento de Física, Facultad de Ciencias Exactas y Naturales, Universidad de Buenos Aires, Intendente Güiraldes 2160, Pabellón I, Ciudad Universitaria, C1428EHA Buenos Aires, Argentina*
[c] *Department of Molecular Biology, Max Planck Institute for Biophysical Chemistry, Am Fassberg 11, D-37070 Göttingen, Germany*
[d] *Consejo Nacional de Investigaciones Científicas y Técnicas, C1033AAJ Buenos Aires, Argentina*

Received 11 January 2007; revised 8 May 2007; accepted 8 May 2007

Available online 25 May 2007

Edited by Felix Wieland

Abstract The retrograde transport of nerve growth factor (NGF) in neurite-like processes of living differentiated PC12 cells was studied using streptavidin-quantum dots (QDs) coupled to monobiotin-NGF. These reagents were active in differentiation, binding, internalization, and transport. Ten-35% of the QD–NGF–receptor complexes were mobile. Quantitative single particle tracking revealed a bidirectional step-like motion, requiring intact microtubules, with a net retrograde velocity of 0.054 ± 0.020 μm/s. Individual runs had a mean velocity of ~0.15 μm/s at room temperature, and the run times were exponentially distributed. The photostability and brightness of QDs permit extended real-time analysis of individual QDbNGF–receptor complexes trafficking within neurites.

Keywords: Live cell imaging; Neurotrophins; NGF; Retrograde axonal transport; Quantum dots

1. Introduction

The neurotrophin NGF is a peptide dimer of 26 kDa responsible for the regulation of survival, differentiation and maintenance of responsive neurons. It is produced and released from target tissues and interacts with receptors on the tips of axons [1,2]. For neurotrophins to mediate survival, they must have the ability to transduce a series of complex signaling events from the terminal plasma membrane of a nerve to the nucleus situated in the cell body. Responses to NGF are mediated by two classes of receptors: p75 and TrkA. According to the signaling endosome model [3–5], NGF is bound to its receptors on the membrane surface, is endocytosed via the clathrin-mediated endocytic pathway, and then transported from the axon terminus to the soma by interaction with different components of the cytoskeleton machinery [6–9]. The NGF–receptor complexes activate different signaling scaffolds depending on their nature and endosomal localization. Activation of these cascades leads to cellular responses that range from differentiation and survival to apoptotic cell death. Numerous aspects regarding the formation and nature of the signaling complexes and how these complexes are processed remain unclear. Resolution of these questions is of fundamental importance for understanding normal and pathological processes in the nervous system.

The aim of the present work was to employ new imaging reagents and technology to characterize the biophysical behavior of retrograde transport of NGF in living cells and in real time. Recently, Tani et al. [10] reported the binding and internalization of Cy3-NGF at the single molecule level in DRG growth cones but could only track the NGF for very short times due to photobleaching of the fluorescent label. Vu et al. showed that bNGF associated with fluorescent nanoparticles bound to and promoted differentiation of PC12 cells [11]. In this work, we followed NGF trafficking inside neurites of differentiated PC12 cells by tracking trace amounts of streptavidin-coated quantum dots bound to biotinylated NGF (bNGF). Quantum dots (QDs) are brightly fluorescent nanometer-scale semiconductor crystals; their extreme photostability render them ideal probes for cellular imaging over extended time periods, as we and others have demonstrated in studies of receptor-mediated signaling in living cells [12–18]. Using this strategy we visualized NGF binding, internalization and trafficking in the neurite-like processes of PC12 cells and characterized the kinetics of the NGF trafficking process in previously unattained detail. The QD ligands revealed that the movement of the cytoskeleton-associated receptor complexes is bidirectional, but that net transport toward the cell body arises from statistically longer run lengths in the retrograde direction.

2. Materials and methods

2.1. Reagents

All reagents were of analytical grade. Mouse NGF was purchased from Alomone Labs (Jerusalem, Israel). Streptavidin-conjugated

*Corresponding author. Fax: +54 11 4576 3426.
E-mail address: lia@df.uba.ar (L.I. Pietrasanta).

Abbreviations: NGF, nerve growth factor; bNGF, monobiotin-NGF; QDs, quantum dots

0014-5793/$32.00
doi:10.1016/j.febslet.2007.05.041

655 nm pegylated and 605 nm non-pegylated quantum dots (QDs) (~80 nm FWHM) were purchased from Quantum Dot Corp. (Invitrogen). Media and sera for cell culture were from Invitrogen. Tyrode's buffer: 135 mM NaCl, 10 mM KCl, 0.4 mM $MgCl_2$, 1 mM $CaCl_2$, 5.6 mM glucose, 0.1% (w/v) BSA and 10 mM Na-HEPES (pH 7.4).

2.2. Cell culture

PC12 cells (gift of Dr. F. Bronfman, Catholic University of Chile) were grown in Dulbecco's modified Eagle's medium (DMEM) containing glutamine, high glucose, 6% horse serum, 6% fetal calf serum and 100 U/ml penicillin–streptomycin (complete media). Differentiation was induced by the addition of 2 nM NGF or mono-biotinylated NGF in complete media to cells seeded on 12 mm coverslips coated with poly-D-lysine (see Supplementary Fig. S1). No difference was discerned in the differentiation kinetics associated with NGF or bNGF. In most experiments NGF was used to induce differentiation for 3–4 days and was exchanged for bNGF at least 1 h before addition of QDs.

2.3. bNGF synthesis

NGF was biotinylated according to the method of Bronfman et al. [19] modified so as to maximize the yield of single labeled molecules. [NGF carrying multiple biotins (~9) was also active but induced the binding of aggregated QDs to the surface of the PC12 cells and impaired internalization kinetics. Such preparations were not used in the studies presented here.] Biotinylation reagents were purchased from Pierce. NGF (0.5 mg) was incubated in the presence of 30 mM EDC and 25 mM of EZ-link biotin-PEO-amine in 0.1 M Na-MES buffer (pH 5.0) for 2 h at room temperature. Biotinylated NGF (bNGF) was separated from the reaction mixture by reverse phase HPLC using a Vydac C8 column (Grace-Vydac) with an acetonitrile/water/trifluoroacetic acid gradient. The bNGF was characterized by spectroscopy and MALDI-TOF (Bruker Reflex 4 Scout 384) and functional analysis for promoting PC12 cells differentiation as described in Section 2.2.

2.4. Calibration of quantum dot signals

A 100 pM QD solution was deposited on a slide and visualized by fluorescence microscopy (see Supplementary Fig. S2 A, B). To determine the intensities of QDs, the total intensity of a small ROI containing each QD was measured. The distribution of the intensities obtained in this way peaked at a value of ~15 000 photons/s. A few loci, presumably representing clusters of QDs, exhibited higher intensities (see Supplementary Fig. S2 C). The time courses of the mean intensity of single spots (total intensity/number of pixels in the ROI) showed the typical blinking behavior (blue line in Supplementary Fig. S2 D) indicative of single QDs [20]. Blinking did not extinguish the fluorescence of the more intense spots (lines red and green in Supplementary Fig. S2 D). Similar results were obtained for the preformed 1:1 QD–bNGF complexes, indicating that the binding of bNGF neither induced nor increased QD aggregation. These distinctions in intensity distribution and blinking behavior were used to distinguish between single and multiple QDs bound to and internalized in living cells.

2.5. QD labeling

Differentiated PC12 cells were treated with 2 nM bNGF in complete media without phenol red at 37 °C during 1 h, washed and exposed to 50 or 500 pM QDs in Tyrode's buffer at 37 °C for 15 min. The cells were then washed three times with Tyrode's buffer and mounted on a silicon or a flow chamber with DMEM containing 5% horse serum and 2 nM NGF for imaging at room temperature. For the internalization experiments, the cells were incubated at 37 °C in complete media containing 2 nM NGF for various time periods before imaging.

2.6. Acid treatment

PC12 cells were incubated for 1 min with a solution containing 0.1 M acetic acid, 150 mM choline chloride and 0.1% FCS at room temperature followed immediately by complete medium.

2.7. Nocodazole treatment

PC12 cells were labeled and imaged at room temperature in a flow chamber. After 10–20 min of imaging, the medium was replaced by complete medium containing 2 nM NGF and 20 μM nocodazole, incubated for 30 min with imaging.

2.8. Microscopy

Images were acquired with an Axioskop2Mot Zeiss microscope and an Apogee U2000 CCD camera using MaxIms DL v.3.21 software. For QD visualization, a C-Apochromat 63 × (NA 1.2) water immersion objective, BP546 excitation, 580 nm dichroic, and QD specific emission filters (Chroma Technology Corp.) were used.

2.8.1. Image acquisition. Live cell QD tracking on neurites was performed by acquisition of a time series of 512 × 512 pixel images with a pixel resolution of 0.12 μm/pixel, an integration time of 0.5–1 s and intervals between images of 0 and 1 s.

2.8.2. Image analysis. The positions of QDs in x and y were tracked using ImageJ v.1.34 routines (NIH, Bethesda, MA) after selection of an ROI from the image series that contained no more than 4–5 QDs. The x and y coordinates were further processed with routines implemented in Matlab (The MathWorks Inc.). For neurite images two principal axes were defined from the DIC image: one parallel (y) and the other perpendicular (x) to the direction of the neurite. The data points were rotated, rewritten and movements in both directions were studied independently. Kymographs were constructed with the View5D Image J plug-in (http://wwwuser.gwdg.de/~rheintz/View5D), superposing y vs. time plots for x positions lying within a range corresponding to the width of the neurites, thereby compensating for x fluctuations.

2.8.3. Trajectory analysis. Run lengths and times of run were determined by visual inspection from individual time courses of positions in the parallel (y) direction. The criterion chosen to establish the existence of a run was the alignment of four or more successive data points. The velocity of an individual run was determined as the ratio of the length and corresponding duration of the run.

3. Results

3.1. Specificity and selectivity of QD binding to bNGF-labeled PC12 cells

The neurite-like processes of PC12 cells, induced to differentiate by treatment with NGF for several days, constitute a model system for the study of the behavior of NGF–receptors. We selected photostable QD-coupled ligands to perform long-term in vivo observations of the NGF–receptors. Treatment of differentiated PC12 cells with 500 pM pegylated, streptavidin-conjugated QDs showed neither binding to cells nor to the poly-D-lysine coated substrate as is seen in Fig. 1C. [We caution against the use of non-pegylated QDs which present some affinity for the positively charged substrate (data not shown)]. We synthesized a predominantly mono-biotinylated NGF (bNGF) (see Section 2), which behaved identically to non-biotinylated NGF with respect to the induction of differentiation of PC12 cells (Supplementary Fig. S1). In order to generate a cohort of QD–bNGF–receptor complexes suitable for tracking we labeled primed, differentiated PC12 cells with 2 nM bNGF for at least 1 h at 37 °C and subsequently added QDs at various concentrations for 15 min. As seen in Fig. 1C, 500 pM QDs bound extensively to the cell body and single receptor complexes were difficult to distinguish at these concentrations. A short (15 min) incubation with 50 pM QDs optimally labeled bNGF-primed, differentiated PC12 cells, such that we could subsequently track individual endocytosed receptor complexes in the neurites (Fig. 1D–I).

3.2. Internalization of QD–bNGF complexes

The rate of internalization of QD–bNGF complexes was quantified by comparing the total fluorescence intensity of the QD signal before and after acidic treatment leading to the removal of externally bound complexes [21]. Differentiated PC12 cells primed with bNGF were incubated with 50 pM 655 nm QDs for 15 min. Unbound QDs were removed by

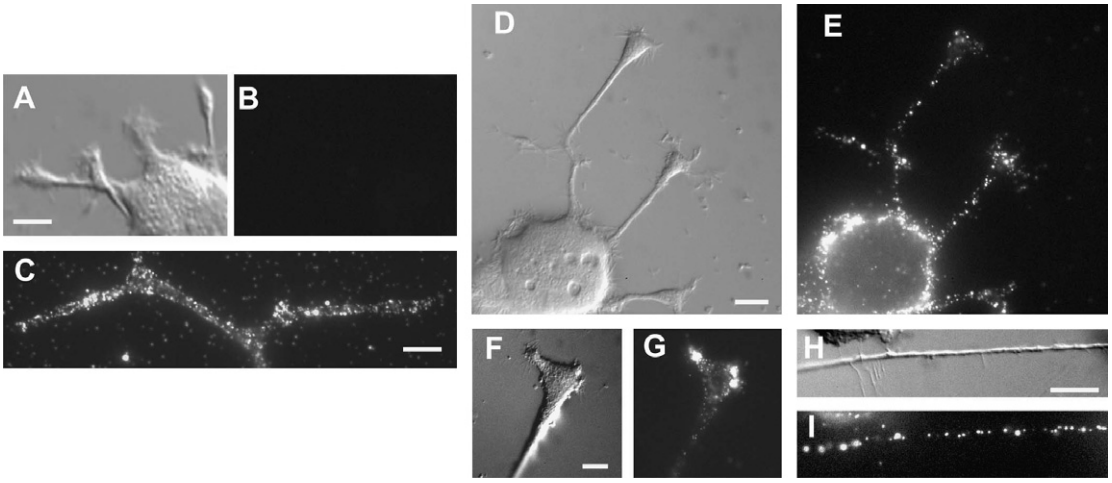

Fig. 1. QD binding to bNFG–receptors and their distribution on PC12 cells. Differentiated PC12 cells were sequentially labeled with bNGF and 655 nm QD at 500 pM (C) or at 50 pM (A–B, D–I). (A, B) Image control of a PC12 cell incubated with NGF prior to QDs addition. (D, E) Image of an entire bNGF-primed PC12 cell labeled with 50 pM 655 nm QDs. (F, G) Detailed image of a growth cone. (H, I) Detailed image of a neurite of the same preparation. DIC images: A, D, F and H. Fluorescence images, B, C, E, G and I, were obtained by 450–490 excitation with 655 nm (20 nm HW) emission. Resolution: 0.12 μm/pixel. Scale bar, 10 μm.

washing, and cells were incubated at 37 °C for various time periods in complete media containing 2 nM NGF. At the indicated time points (Fig. 2) cells were imaged before and after treatment with 0.1 M HOAc. Fig. 2A shows representative images for three time points. The zero time point was determined by incubation with QDs at 0 °C, and imaging was performed before and after acid wash without exposure to 37 °C. The internalization time course is plotted in Fig. 2B as the ratio of the fluorescent signals after and before exposure to acid. Internalization reached a plateau after 1 h at 37 °C. These results are in good agreement with published observations based on bulk experiments using radioactively labeled ligand [22–25]. We conclude that the QD–bNGF reagent exhibits the properties of unmodified neurotrophin.

3.3. QD–bNGF trafficking kinetics on PC12 neurite outgrowths

The photostability of QDs permitted the prolonged imaging in real time of QD–bNGF–receptor trafficking in neurite-like processes of PC12 differentiated cells. Fig. 3A shows selected time points from a series of in vivo images of the fluorescent signals in a PC12 neurite. Some loci migrated from the neurite terminal toward the cell body (i.e. from right to left) depicted by yellow and red arrows, while others remained stationary or fluctuated around their original position (yellow and red asterisks; see also Supplementary Movie 1 and 2). A representative kymograph of the intensities measured in an ROI along a neurite is shown in Fig. 3D. (Further examples may be seen in Supplementary Fig. S3). One can distinguish clearly the intensity traces of both stationary and moving QDs. In all experiments we observed that only a fraction (10–35%) of the total number of QD–bNGF complexes displayed retrograde motion. Our results are compatible with those of Ure and Campenot [26], who reported that after steady-state binding of radiolabelled NGF, only 5–30% of the axon-bound ligand reached the cell bodies after 15–24 h of incubation. In addition, Tani et al. [10] observed that in the steady state only 17% of the Cy3-NGF complexes showed rearward movement to the central region of DRG growth cones, while the rest underwent diffusive motion.

In order to determine whether the particles were being transported inside or on the surface of the neurites, we tracked QD–bNGF–receptor complexes before and after the acid wash treatment described above. Loci undergoing retrograde transport were immobilized but not removed, whereas some stationary loci disappeared after acid treatment (see a representative experiment in Supplementary Fig. S4). We conclude that all retrograde trafficking of QD–receptor complexes takes place inside the neurite.

The nature and kinetics of transport of QD–bNGF–receptor complexes were analyzed in detail by tracking the movements of single QD loci within cell neurites over time and at high resolution. Fig. 4 shows the tracks of such loci, MSD plots of their net displacements in y, and a 3D plot (panel A) of the positions of the particles during the tracking time for a moving (in blue) and immobile (in red) locus in a PC12 process. The initial positions were arbitrarily defined for the sake of figure clarity. The motion towards negative y values represented retrograde motion.

The net movements of the complexes were unidirectional along the neurite principal axis, showing stepwise behavior in y and fluctuations in the transversal (x) axis. This behavior is clearly seen in plots of particle trajectories independent of time (x–y plot, Fig. 4B). The moving particle in Fig. 4A and B traversed a total distance of 8 μm in the retrograde direction during 150 s of tracking. The mean transversal displacement was negligible (2 nm). The maximal amplitude in any track measured in this direction was ~1.5 μm (the mean neurite diameter was 1.6 μm).

Fig. 4C shows trajectories of several loci. Fitting a linear equation to the y vs. time data provided an estimate of the mean velocity for the directed motion toward the cell body of 0.058 ± 0.014 μm/s (mean ± S.D., n = 11). Due to the discontinuous nature of the transport process, the determination of the mean velocity depends on the method of analysis: if pausing and backward motions are considered, the computed mean velocity will be lower than for cases in which only net advance (runs) is taken into account. For the retrograde runs, the calculated mean velocity was 0.15 μm/s, a value in the range of

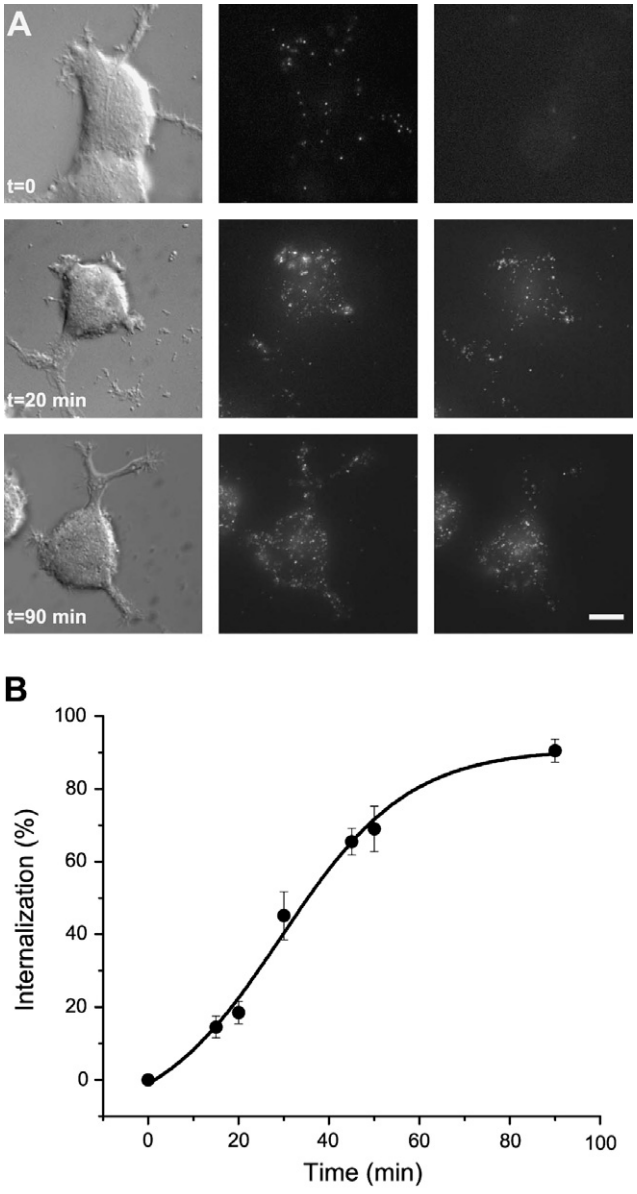

Fig. 2. Internalization of bNGF–QD-complexes at 37 °C. (A) DIC and fluorescence images of cells that were sequentially labeled with bNGF and 655 nm QD, incubated for different time periods and washed with acidic medium. Left column, DIC; middle and right columns, fluorescence before and after acid wash, respectively. The fluorescence images represent the projections of different focal planes spanning the whole cell height. Resolution: 0.12 μm/pixel. Scale bar, 10 μm. (B) Internalization time course plot. Internalization percentages calculated as the ratio between QD–bNGF that remained after acidic treatment and the initial QD–bNGF signal are plotted as a function of time.

the transport velocities of 0.2–2 μm/s reported from bulk experiments using I^{125}-NGF [27]. Tani et al. calculated a rate of 0.06 μm/s for the transport of Cy3-NGF on actin filaments in DRG growth cones at 37 °C.

Mean square displacements (MSD) were calculated for moving particles and plotted as a function of time (Fig. 4D). They displayed the upward curvature indicative of directed motion. The absolute velocity v calculated from a fit of the quadratic function (MSD = $v^2\,\Delta t^2$) to the data in Fig. 4D (red line traces) yielded a value of 0.054 ± 0.020 μm/s (n = 11). Inspection of the particle tracks from several experiments revealed the presence of some tracks with highly processive behavior and others where reversals were more common (Fig. 4B). By analyzing moving and resting periods we determined that moving particles were engaged in retrograde motion for ~60% of the time.

The MSD analysis of QD–bNGF motion is compatible with a facilitated transport process. Biochemical and molecular biology data have demonstrated a direct interaction of TrkA and TrkB with dynein, and retrograde transport of neurotrophin-stimulated cells is abrogated upon inhibition of dynein motors [9,28,29]. The retrograde velocities of QD–bNGF complexes were in the range of those found for dynein and kinesin mediated receptor transport on microtubule networks in vivo at 25 °C but slower than those reported from measurements at 37 °C [13,30,31]. Furthermore, the step-like transport behavior of the QD–bNGF complexes is similar to that observed in vivo and in vitro for the trafficking of vesicles or beads on microtubules mediated by dynein [32–37].

One can interpret the retrograde motion in terms of run lengths, that is, the distances traveled without perceptible pauses or reversals of direction. A representative time course showing runs in the retrograde (blue) and anterograde (red) direction is displayed in Fig. 5A. Panel 5B shows a plot of run length vs. the duration of the runs determined in 11 independent trajectories. The run lengths were highly variable, with run times more variable for longer lengths, probably due to masking of short pauses by the finite image acquisition times. Within the track of a single particle (see Supplementary Fig. S5) the correlations between run length and run time for the retrograde and anterograde runs were similar. These plots also suggest that the net retrograde displacement resulted from runs proceeding further and for longer time periods in the retrograde direction. Fig. 5C, a plot of velocity vs. the duration of the same runs as in Fig. 5B, reveals that more particles exhibited larger velocities in the retrograde than in the anterograde direction. It also demonstrates that high velocities were not maintained for long time periods; that is, only a few loci were capable of fast, sustained motion.

The histograms of anterograde and retrograde run lengths captured from the same trajectories (Fig. 5D) exhibited maxima between 0.5 and 1 μm. (Our acquisition system limited the resolution of this analysis to 0.5 μm). In agreement with Fig. 5B, more particles moved in the retrograde than in the anterograde direction and reached longer distances. An exponential decay was also observed for the run times of these particles (see histogram in Fig. 5E). Most of the runs corresponded to velocities of ~150 nm/s in both directions, although more runs were directed toward the cell body (Fig. 5F).

Experiments in vitro have demonstrated that microtubule motors travel over only limited distances because of the finite probability of detachment at each step [38]; the mean distance is ~1.4 μm. A plot of run lengths for vesicular transport in vivo showed an exponential distribution with a mean length of ~1 μm [33] in *Drosophila* embryos and 1.3 μm [37] in PC12 cells. We observed a similar behavior for the run lengths shown in Fig. 5, for which the mean travel distance was ~1 μm for both retrograde and anterograde runs.

From the observed decrease in the persistence of motion over time, we infer that the QD–bNGF complexes were coupled to a motor protein with limited processivity. The particles

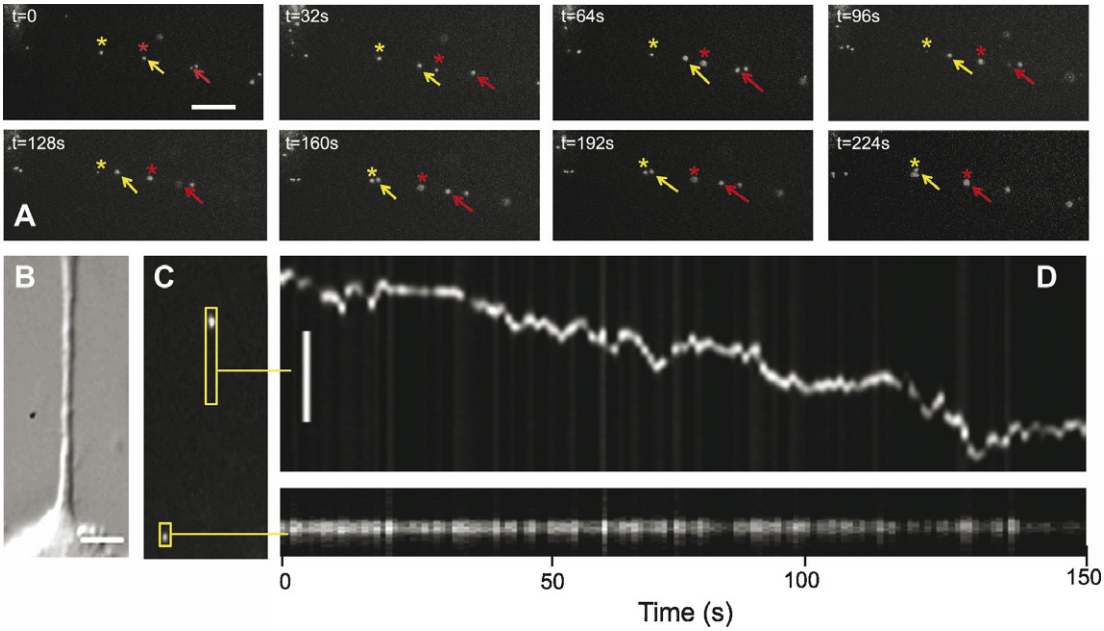

Fig. 3. QD–bNGF complexes trafficking within a neurite-like process. (A) 8 of 135 frames (exposure time, 0.7 s; time between images, 1 s) of a tracking experiment. Complexes that moved (yellow and red arrows) from the end of the process toward the cell body (upper left side in each image), complexes that remained in the same place during the acquisition time (yellow and red asterisks). Scale bar, 10 μm. (B, C) DIC and fluorescence images of a different neurite labeled with QD–bNGF during a tracking experiment. Scale bar, 5 μm. (D) Kymograph of the ROIs depicted in Fig. 3C. Images were taken every second. The cell body was located downwards. A moving QD–bNGF complex (upper panel) traveled 8 μm during 150 s of tracking towards the cell body. Scale bar 5 μm. Resolution: 0.12 μm/pixel. Movies of the extended times series for C from which the kymographs were extracted are available as Supplementary Movies 1 and 2.

exhibited different run velocities during their trajectories, with a mean of ~0.15 μm/s for both directions, suggesting that these different velocities could be explained by changes in the number of attached motors per run [37]. Fluctuations in the transverse direction of motion may also be explained by a dynein-mediated transport process, in which the dynein may jump between microtubule protofilaments while moving in the retrograde direction [32].

3.4. QD–bNGF–receptor complexes transport requires intact microtubules

Dynein is a molecular motor that translocates on microtubules, the integrity of which must be mantained in order that receptor signals reach the cell body [27]. To assess if QD–bNGF–receptor complexes were being transported by the same molecular machinery as native NGF, we tested the effect of the microtubule disrupting agent, nocodazole, on the trafficking of QD-complexes by imaging a given cell before and after treatment with this agent. Fig. 6 shows the kymographs of two independent tracking experiments in a time window just prior to seeing an effect of the drug (about 30–40 min after addition of the drug). Transport velocities similar to untreated cells were abruptly terminated at ~30 min after addition of nocodazole, a result consistent with the dependence of transport on intact microtubules. No directed movement was observed after arrest (indicated by an asterisk) in the presence of the drug.

4. Discussion

Neurotrophins are usually released at neurite growth cones whereas downstream transcriptional signaling occurs in the cell body, thus necessitating a mechanism for transporting signals (molecules) along the length of the intervening axon. Numerous biochemical studies based on radioactively labeled NGF have demonstrated NGF uptake and transport in tissues and neuronal cultures [8,26]. It has been proposed that following clathrin-mediated NGF uptake, vesicular retrograde transport of the receptor–ligand complex occurs along microtubules [5,8,39]. Most organelles use both plus-end directed kinesins to carry cargo to the cell periphery and minus-end directed dynein to bring cargo back [40–42]. Immunochemical and inhibition experiments have implicated both dynein and kinesin in NGF–receptor vesicular trafficking [28,43].

In a previous study, Lalli and Schiavo [31] visualized NGF retrograde transport in living motor neurons and recently, Tani et al. [10] characterized the uptake of NGF in living DRG growth cones using Cy3-labeled NGF. In this study we greatly extended the temporal window of observation by introducing the use of quantum dots (QDs) to tag biotin-NGF bound to surface receptors on living differentiated PC12 cells. We modified the biotinylation protocol to achieve a predominantly mono-biotinylated adduct of NGF, which was fully functional in the differentiation of PC12 cells at concentrations used normally for unmodified NGF. The binding and kinetics of endocytosis of QD–bNGF on primed, differentiated PC12 cells were specific. Imaging of individual and clustered QD–bNGF complexes in real time in live cells enabled us to analyze the in situ kinetics of NGF transport in PC12 axonal-like neurites. Although any label/probe has the potential for perturbing the properties and function of the conjugated ligand, other studies have shown that QD-labeled ligands retain biological function [11–14] and the data presented here demonstrated similar uptake kinetics for complexes of QD–bNGF and of native NGF with NGF–receptors. Such results are in

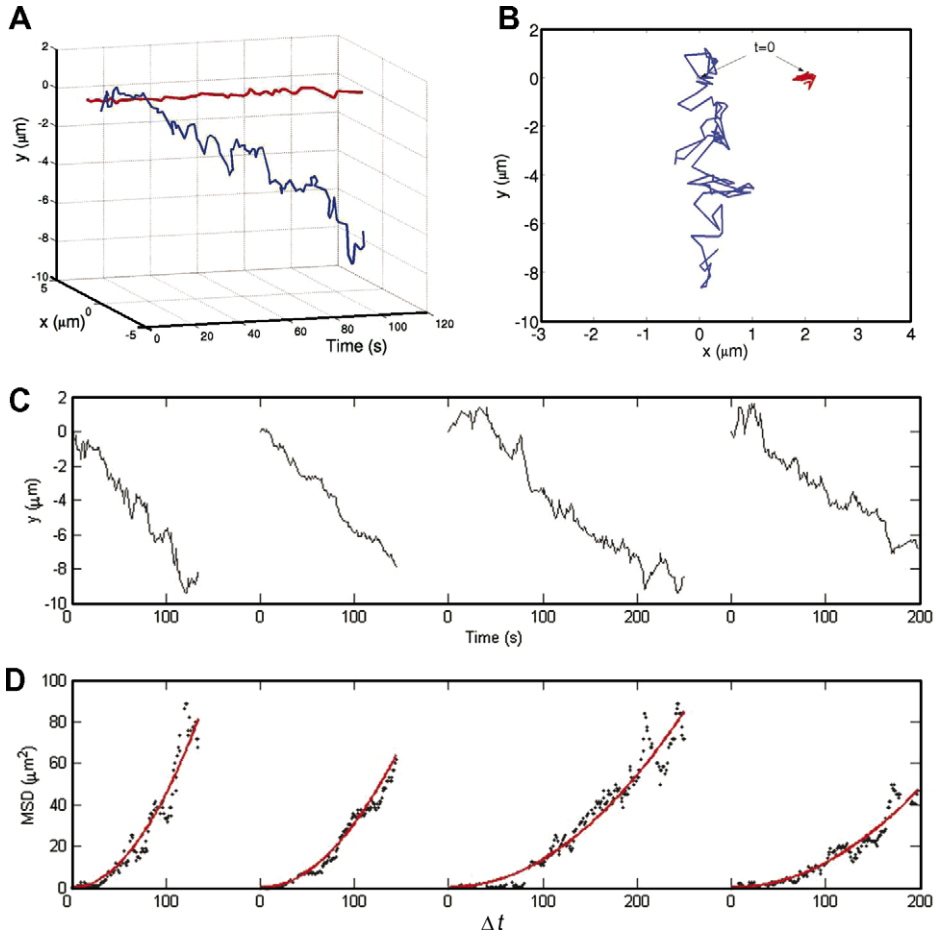

Fig. 4. Kinetic analysis of QD–bNGF complex transport. (A, B) Spatial-temporal 3D graph and y vs. x plot, respectively, of the moving (blue) and immobile (red) loci from Fig. 3D. (C) Trajectories (y vs. time plots) of loci recorded in four independent experiments. (D) MSD vs. time displacements (Δt) traces shown in panel C. Red line, fit to the equation MSD = $v^2\Delta t^2$ of the data.

agreement with published observations based on bulk experiments and radioactively labeled NGF [22,24,25,35] but extend them to single molecule sensitivity with direct observations over long time periods due to the extraordinary photostability of QDs. During the preparation of this manuscript, Rajan and Vu [44] showed that antibody-coupled QDs were bound to the TrkA receptor and underwent retrograde movement to the cell body. However, vesicular tracking was performed for short times, i.e. <90 s and no data were presented as to whether these antibody complexes were also associated with NGF-activated receptors.

We observed a net retrograde transport of QD–bNGF complexes and demonstrated that the transporting molecules were not removed by acid treatment, thereby indicating that they had been internalized. Like many cytoplasmic organelles, QD–bNFG–receptor complexes exhibited bidirectional movement along microtubules after endocytosis [33]. From quantitative analysis of the tracking data, we derived rates and extents of transport in both the retrograde and anterograde directions. Taking into consideration only the mobile population of QD-labeled, endocytosed receptors, we characterized the retrograde movement as a broken "staircase structure", with regions of net advance, pauses, and reversals (see Fig. 4). The net displacement was biased in the direction of the cell body, i.e., retrograde. On average, the QDs moved ~70% of the time, and 60% of this movement was directed towards the cell body. The velocities in the two directions, were very similar and only the run lengths seem to be biased in the retrograde direction. In addition, pauses were often quite short. A dynein-mediated transport mechanism has been suggested by other cellular and molecular biological studies of TrKs receptors [9,28,29,43]. Recently, Ross et al. [45] demonstrated that purified dynein–dynactin complexes in vitro move bidirectionally on taxol stabilized, polymerized microtubules. In that study signals were followed for 20 s or less and most tracks were recorded for only 4 s. Nonetheless, these results support our interpretation of the transport in neurites by a single type of motor protein.

Bidirectional transport is a process exhibited by many organelles [mitochondria, pigment in fish and frogs, lipid droplets, secretory vesicles and endosomes (for references see Gross, 2004 [33]) and has been studied extensively. Nan et al. reported bidirectional lysosomal trafficking 12 h after internalization of non-specific Arg_9 linked QD aggregates [46]. Our results provide new and important insights into the trafficking of NGF in neurites. Although biochemical and molecular biology experiments have demonstrated the association of dynein to Trk receptors, this is the first report that characterizes the transport of a subpopulation of NGF–receptor complexes by association with a processive, bidirectional

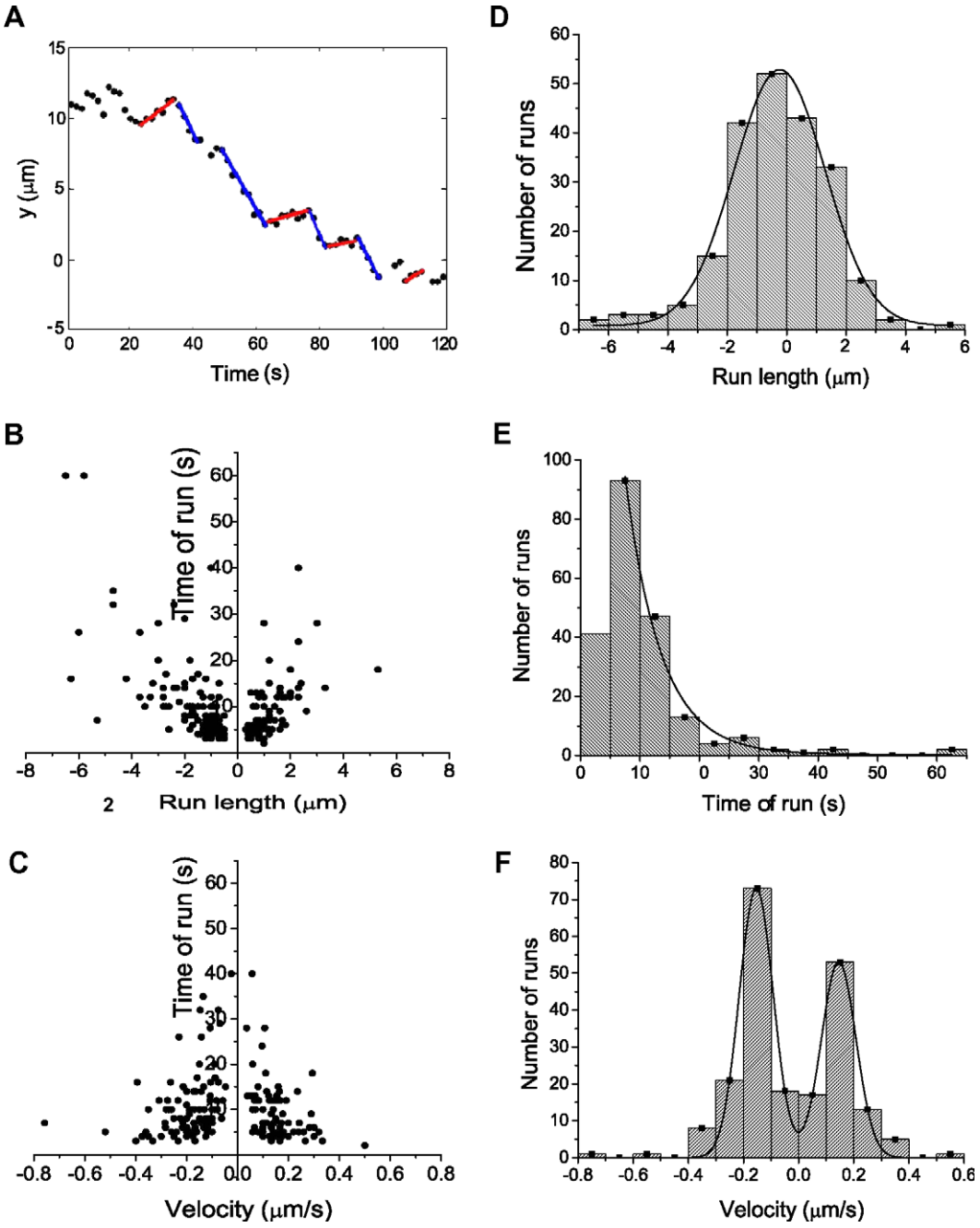

Fig. 5. Analysis of the transport behavior of QD–bNGF complexes. (A) Representative *y* vs. time plot showing retrograde (blue) and anterograde (red) runs (1.67 s/frame). 2-D correlation between run length and time (B) and velocities and time (C) for the trajectories determined in 11 independent tracking experiments. Distributions of run lengths (D); durations of runs (E); and velocities (F) for the data plotted in B and C.

motor. A vast literature exists based on short time experiments in which steps of molecular motors were characterized. Nevertheless, such data do not exist (to our knowledge) for long-term processes such as the transport of NGF in neuronal cells. It has been stated in the literature [10,33] that typical run lengths for motor-mediated transport are on the order of 1 μm and mean velocities range between 0.06 μm/s [10] and 2 μm/s [27], from which one may conclude that processive motion is maintained for only a few seconds. Thus, although our time resolution did not allow us to resolve (“see”) single motor steps, it permitted observation over physiologically relevant temporal and spatial scales. We are currently employing advanced optical sectioning techniques coupled with very sensitive detection using electron multiplying CCD cameras to significantly extend the time resolution of such determinations.

The new information gained through single particle (and thus single molecule) tracking were possible due to the unique properties, particularly photostability, of the quantum dot nanoparticles [14,47] and would have been unachievable using conventional organic fluorophores (due to limited photostability), or micron-seized beads (due to size restrictions). We anticipate further insights into the detailed molecular machinery of axonal retrograde transport by application of these techniques to primary neuronal preparations.

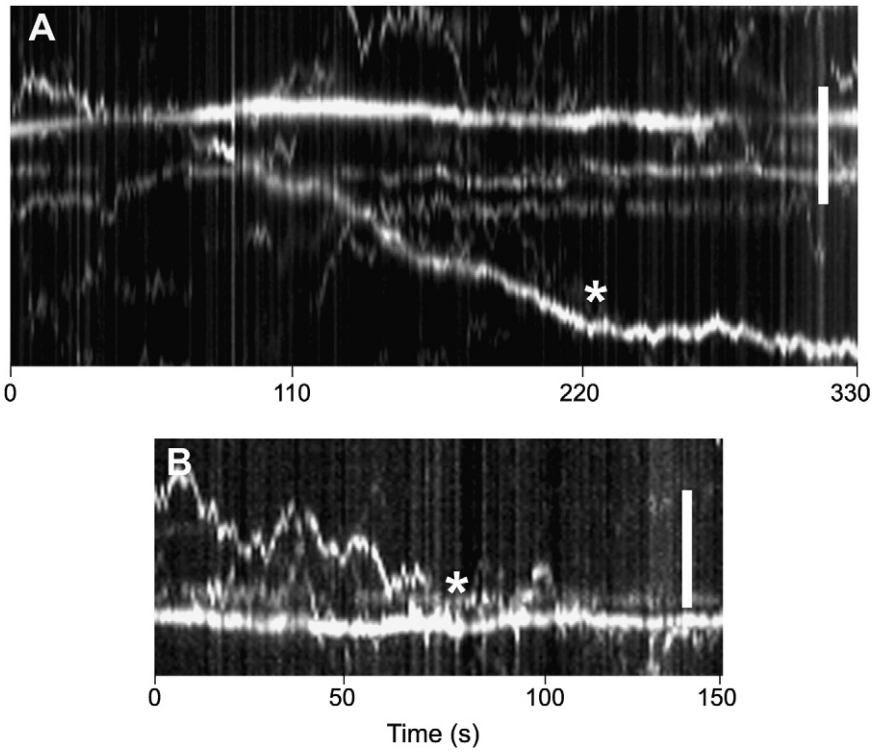

Fig. 6. Effect of nocodazole treatment. (A, B) Kymographs of two independent tracking experiments. Trajectories starting ~30 min post nocodazole treatment. Asterisks, times at which the particles stopped. Resolution: 0.12 μm/pixel. Scale bar 5 μm.

Acknowledgments: We are grateful to Dr. L. Alché for the use of cell culture facilities and for helpful discussions. We thank Dr. F. Bronfman for generous provision of the PC12 cell line and advice regarding experimental design, Dr. E. Jares-Erijman and Lic. C. Spagnuolo for their assistance with NGF labeling, Lic. H. Grecco for suggestions on image analysis, Dr. H. Urlaub (MPIbpc) for MALDI-TOF analysis of biotin-NGF. This work was carried out under the auspices of a BMBF (Germany)-MOS (Israel) funded collaboration between the Center for Advanced Microscopies, FCEyN-UBA, Argentina, the Department of Molecular Biology of the Max Planck Institute for Biophysical Chemistry (MPIbpc), Germany, and the Molecular Neurobiology Group, Weizmann Institute of Science, Israel. A Fundación Antorchas postdoctoral fellowship was awarded to M.M.E. and CONICET postdoctoral fellowships to M.M.E., and L.B.

Appendix A. Supplementary data

Supplementary data associated with this article can be found, in the online version, at doi:10.1016/j.febslet.2007.05.041.

References

[1] Levi-Montalcini, R. (1987) The nerve growth factor 35 years later. Science 237, 1154–1162.
[2] Yuen, E.C. and Mobley, W.C. (1995) Therapeutic applications of neurotrophic factors in disorders of motor neurons and peripheral nerves. Mol. Med. Today 1, 278–286.
[3] Campenot, R.B. and MacInnis, B.L. (2004) Retrograde transport of neurotrophins: fact and function. J. Neurobiol. 58, 217–229.
[4] Di Fiore, P.P. and De Camilli, P. (2001) Endocytosis and signaling: an inseparable partnership. Cell 106, 1–4.
[5] Delcroix, J.D., Valletta, J.S., Wu, C.B., Hunt, S.J., Kowal, A.S. and Mobley, W.C. (2003) NGF signaling in sensory neurons: evidence that early endosomes carry NGF retrograde signals. Neuron 39, 69–84.
[6] Grimes, M.L. et al. (1996) Endocytosis of activated TrkA: evidence that nerve growth factor induces formation of signaling endosomes. J. Neurosci. 16, 7950–7964.
[7] Hendry, I.A. and Iversen, L.L. (1973) Reduction in concentration of nerve growth factor in mice after sialectomy and castration. Nature 243, 500–504.
[8] Hendry, I.A., Stockel, K., Thoenen, H. and Iversen, L.L. (1974) Retrograde axonal transport of nerve growth factor. Brain Res. 68, 103–121.
[9] Vallee, R.B., Shpetner, H.S. and Paschal, B.M. (1989) The role of dynein in retrograde axonal transport. Trends Neurosci. 12, 66–70.
[10] Tani, T., Miyamoto, Y., Fujimori, K.E., Taguchi, T., Yanagida, T., Sako, Y. and Harada, Y. (2005) Trafficking of a ligand–receptor complex on the growth cones as an essential step for the uptake of nerve growth factor at the distal end of the axon: a single-molecule analysis. J. Neurosci. 25, 2181–2191.
[11] Vu, T.Q., Maddipati, R., Blute, T.A., Nehilla, B.J., Nusblat, L. and Desai, T.A. (2005) Peptide-conjugated quantum dots activate neuronal receptors and initiate downstream signaling of neurite growth. Nano Lett. 5, 603–607.
[12] Lidke, D.S., Lidke, K.A., Rieger, B., Jovin, T.M. and Arndt-Jovin, D.J. (2005) Reaching out for signals: filopodia sense EGF and respond by directed retrograde transport of activated receptors. J. Cell Biol. 170, 619–626.
[13] Lidke, D.S., Nagy, P., Heintzmann, R., Arndt-Jovin, D.J., Post, J.N., Grecco, H.E., Jares-Erijman, E.A. and Jovin, T.M. (2004) Quantum dot ligands provide new insights into erbB/HER receptor-mediated signal transduction. Nat. Biotechnol. 22, 198–203.
[14] Dahan, M., Levi, S., Luccardini, C., Rostaing, P., Riveau, B. and Triller, A. (2003) Diffusion dynamics of glycine receptors revealed by single-quantum dot tracking. Science 302, 442–445.
[15] Smith, A., Gao, X. and Nie, S. (2004) Quantum-dot nanocrystals for in vivo molecular and cellular imaging. Photochem. Photobiol. 80, 377–385.

[16] Lehmann, M.J., Sherer, N.M., Marks, C.B., Pypaert, M. and Mothes, W. (2005) Actin- and myosin-driven movement of viruses along filopodia precedes their entry into cells. J. Cell Biol. 170, 317–325.
[17] Gao, X., Yang, L., Petros, J.A., Marshall, F.F., Simons, J.W. and Nie, S. (2005) In vivo molecular and cellular imaging with quantum dots. Curr. Opin. Biotechnol. 16, 63–72.
[18] Fu, A., Gu, W., Larabell, C. and Alivisatos, A.P. (2005) Semiconductor nanocrystals for biological imaging. Curr. Opin. Neurobiol. 15, 568–575.
[19] Bronfman, F.C., Tcherpakov, M., Jovin, T.M. and Fainzilber, M. (2003) Ligand-induced internalization of the p75 neurotrophin receptor: a slow route to the signaling endosome. J. Neurosci. 23, 3209–3220.
[20] Grecco, H.E., Lidke, K.A., Heintzmann, R., Lidke, D.S., Spagnuolo, C., Martinez, O.E., Jares-Erijman, E.A. and Jovin, T.M. (2004) Ensemble and single particle photophysical properties (two-photon excitation, anisotropy, FRET, lifetime, spectral conversion) of commercial quantum dots in solution and in live cells. Microsc. Res. Tech. 65, 169–179.
[21] Buxser, S., Decker, D. and Ruppel, P. (1990) Relationship among types of nerve growth factor receptors on PC12 Cells. J. Biol. Chem. 265, 12701–12710.
[22] Bernd, P. and Greene, L.A. (1984) Association of I125 nerve growth factor with PC12 pheochromocytoma cells: evidence for Internalization via high-affinity receptors only and for long-term regulation by nerve growth factor of both high-affinity and low-affinity receptors. J. Biol. Chem. 259, 5509–5516.
[23] Jullien, J., Guili, V., Reichardt, L.F. and Rudkin, B.B. (2002) Molecular kinetics of nerve growth factor receptor trafficking and activation. J. Biol. Chem. 277, 38700–38708.
[24] Mahadeo, D., Kaplan, L., Chao, M.V. and Hempstead, B.L. (1994) High-affinity nerve growth-factor binding displays a faster rate of association than P140(Trk) binding – implications for multisubunit polypeptide receptors. J. Biol. Chem. 269, 6884–6891.
[25] Zapf-Colby, A. and Olefsky, J.M. (1998) Nerve growth factor processing and trafficking events following TrkA-mediated endocytosis. Endocrinology 139, 3232–3240.
[26] Ure, D.R. and Campenot, R.B. (1997) Retrograde transport and steady-state distribution of I125 nerve growth factor in rat sympathetic neurons in compartmented cultures. J. Neurosci. 17, 1282–1290.
[27] Watson, F.L., Heerssen, H.M., Moheban, D.B., Lin, M.Z., Sauvageot, C.M., Bhattacharyya, A., Pomeroy, S.L. and Segal, R.A. (1999) Rapid nuclear responses to target-derived neurotrophins require retrograde transport of ligand–receptor complex. J. Neurosci. 19, 7889–7900.
[28] Heerssen, H.M., Pazyra, M.F. and Segal, R.A. (2004) Dynein motors transport activated Trks to promote survival of target-dependent neurons. Nat. Neurosci. 7, 596–604.
[29] Yano, H., Lee, F.S., Kong, H., Chuang, J.-Z., Arevalo, J.C., Perez, P., Sung, C.-H. and Chao, M.V. (2001) Association of Trk neurotrophin receptors with components of the cytoplasmic dynein motor. J. Neurosci. 21 (RC 125), 1–7.
[30] Nakata, T., Terada, S. and Hirokawa, N. (1998) Visualization of the dynamics of synaptic vesicle and plasma membrane proteins in living axons. J. Cell Biol. 140, 659–674.
[31] Lalli, G. and Schiavo, G. (2002) Analysis of retrograde transport in motor neurons reveals common endocytic carriers for tetanus toxin and neurotrophin receptor p75NTR. J. Cell Biol. 156, 233–240.
[32] Wang, Z., Khan, S. and Sheetz, M. (1995) Single cytoplasmic dynein molecule movements: characterization and comparison with kinesin. Biophys. J. 69, 2011–2023.
[33] Gross, S.P., Welte, M.A., Block, S.M. and Wieschaus, E.F. (2000) Dynein-mediated cargo transport in vivo: a switch controls travel distance. J. Cell Biol. 148, 945–955.
[34] Hirakawa, E., Higuchi, H. and Toyoshima, Y.Y. (2000) Processive movement of single 22S dynein molecules occurs only at low ATP concentrations. Proc. Natl. Acad. Sci. USA 97, 2533–2537.
[35] Jullien, J., Guili, V., Derrington, E.A., Darlix, J.L., Reichardt, L.F. and Rudkin, B.B. (2003) Trafficking of TrkA-green fluorescent protein chimerae during nerve growth factor-induced differentiation. J. Biol. Chem. 278, 8706–8716.
[36] Mallik, R., Carter, B.C., Lex, S.A., King, S.J. and Gross, S.P. (2004) Cytoplasmic dynein functions as a gear in response to load. Nature 427, 649–652.
[37] Hill, D.B., Plaza, M.J., Bonin, K. and Holzwarth, G. (2004) Fast vesicle transport in PC12 neurites: velocities and forces. Eur. Biophys. J. Biophys. Lett. 33, 623–632.
[38] Block, S.M., Goldstein, L.S.B. and Schnapp, B.J. (1990) Bead movement by single kinesin molecules studied with optical tweezers. Nature 348, 348–352.
[39] Weible, M.W. and Hendry, I.A. (2004) What is the importance of multivesicular bodies in retrograde axonal transport in vivo? J. Neurobiol. 58, 230–243.
[40] Hirokawa, N. and Takemura, R. (2005) Molecular motors and mechanisms of directional transport in neurons. Nat. Rev. Neurosci. 6, 201–214.
[41] Kural, C., Kim, H., Syed, S., Goshima, G., Gelfand, V.I. and Selvin, P.R. (2005) Kinesin and dynein move a peroxisome in vivo: a tug-of-war or coordinated movement? Science 308, 1469–1472.
[42] Levi, V., Serpinskaya, A.S., Gratton, E. and Gelfand, V. (2006) Organelle transport along microtubules in *Xenopus* melanophores: evidence for cooperation between multiple motors. Biophys. J. 90, 318–327.
[43] Bhattacharyya, A., Watson, F.L., Pomeroy, S.L., Zhang, Y.Z.Z., Stiles, C.D. and Segal, R.A. (2002) High-resolution imaging demonstrates dynein-based vesicular transport of activated Trk receptors. J. Neurobiol. 51, 302–312.
[44] Rajan, S. and Vu, T.Q. (2006) Quantum dots monitor TrkA receptor dynamics in the interior of neural PC12 cells. Nano Lett. 6, 2049–2059.
[45] Ross, J.L., Wallace, K., Shuman, H., Goldman, Y.E. and Holzbaur, E.L. (2006) Processive bidirectional motion of dynein–dynactin complexes in vitro. Nat. Cell Biol. 8, 562–570.
[46] Nan, X., Sims, P.A., Chen, P. and Xie, X.S. (2005) Observation of individual microtubule motor steps in living cells with endocytosed quantum dots. J. Phys. Chem. B Condens. Matter Mater. Surf. Interfaces Biophys. 109, 24220–24224.
[47] Alivisatos, P. (2004) The use of nanocrystals in biological detection. Nat. Biotechnol. 22, 47–52.